AGU PUBLICATIONS

JGR

Journal of Geophysical Research: Oceans

RESEARCH ARTICLE

10.1002/2016JC011661

Key Points:
- Mean squared slope measured by buoys responds to wind forcing in 0.4–1.8 h
- The response time depends on wind speed, fetch, atmospheric stability, and wavelength

Supporting Information:
- Supporting Information S1
- Data Set S1

Correspondence to:
D. D. Chen,
ddchen@umich.edu

Citation:
Chen, D. D., C. S. Ruf, and S. T. Gleason (2016), Response time of mean square slope to wind forcing: An empirical investigation, *J. Geophys. Res. Oceans*, *121*, doi:10.1002/2016JC011661.

Received 18 JAN 2016
Accepted 1 APR 2016
Accepted article online 6 APR 2016

© 2016. American Geophysical Union. All Rights Reserved.

Response time of mean square slope to wind forcing: An empirical investigation

David D. Chen[1], Christopher S. Ruf[1], and Scott T. Gleason[2]

[1]University of Michigan, Ann Arbor, Michigan, USA, [2]Southwest Research Institute, Boulder, Colorado, USA

Abstract We present an empirical study of the response time of surface wave mean square slope to local wind forcing using data collected over 11 years by 46 discus buoys moored at a wide variety of locations. The response time is defined as the time lag at which the time dependence of the waves exhibits the highest correlation with that of the local wind speed. The response time at each location is found to be fairly stable, with the time varying between 0.4 and 1.8 h depending on the location. Examination of long-term statistics reveals response time dependencies on wind speed magnitude, fetch, atmospheric stability, and wavelength. With the increasing reliance on satellite microwave remote sensing as a source of wind data, these results provide useful insights and bounds for their use.

1. Background and Motivation

The evolution of ocean surface waves has been the object of study for many decades. However, much effort has been devoted to the study of two wave properties: wave height and peak frequency [e.g., *Young*, 1999; *U.S. Army Coastal Engineering Research Center (CERC)*, 1977]. Wave height is important to mariners, surfers, and coastal engineers. Peak frequency dictates the velocity of the dominant waves, and is therefore critical to the forecasting of the time of arrival of waves at the coast.

The bulk of past studies on the growth of these two quantities has focused on two ideal cases:

1. Temporal steady-state, in which a steady wind blows for a sufficiently long duration. The wave properties can then be described as a function of distance downwind. This case has been termed "fetch-limited" growth [e.g., *Hasselmann et al*., 1973].
2. Spatial steady-state, in which the winds are steady over a sufficiently large distance. The wave properties are then only a function of time. The wind forcing is considered to be a step function starting from calm conditions. This scenario is known as "duration-limited" growth [e.g., *Hwang and Wang*, 2004a].

All present techniques for the remote sensing of ocean surface winds rely on surface wave properties. In particular, the ocean surface roughness is directly related to the scattering cross section measured in active remote sensing and the brightness temperature sensed in radiometry. The surface roughness includes contributions from higher portions of the wave spectrum than those characterizing the wave height or spectral peak. In monostatic scatterometry, the accepted Bragg scattering theory attributes the signal to resonant reflections from waves of select wavelengths. In bistatic remote sensing and radar altimetry, however, the specular and quasi-specular reflection from large scale slopes is believed to be the dominant contributor to the measurement, and so the low-pass filtered mean square slope is the quantity directly relatable to the radar cross section [*Valenzuela*, 1978; *Zavorotny and Voronovich*, 2000]. In both cases, measurements related to mss are assumed to be, indirectly, proxy measurements of the local winds. The response time of the mss to wind is, then, of fundamental importance to these techniques of ocean wind remote sensing.

Although there have been many studies of the mean square slope and the relevant portions of the wave spectrum, from modeling [e.g., *Hwang et al*., 2013], in-situ sensing [e.g., *Hwang and Wang*, 2004b], and remote sensing [e.g., *Cox and Munk*, 1954; *Jackson et al*., 1992] approaches, empirical research on the evolution of mss as a function of fetch or duration has remained scarce. In this paper, we study the temporal evolution of low pass filtered mss in a variety of field conditions over many years––specifically, measurements by 46 National Data Buoy Center (NDBC) buoys are analyzed. The data set ranges from 2004 to 2014, inclusive.

We begin by giving a detailed account of the instrumentation and data processing. We then present the response time statistics, and show how they are correlated with various geophysical quantities. Finally, we discuss the implications of our results, which are limited by the wavelengths on the shorter end, for remote sensing. Comparisons to duration-limited growth predicted by two wave-age dependent wave spectra are also made.

2. Data Source and Processing

2.1. Data Source

The NOAA NDBC operates and maintains moored buoys in the coastal U.S. regions. The 3 m, 6 m, and 10 m discus buoys are capable of measuring the wave frequency spectrum as well as many other environmental parameters such as wind speed, wind direction, air temperature, and sea surface temperature (SST). The majority of the buoys are of the 3 m discus type. The nondirectional wave spectrum is derived from a time series of heave acceleration measurements collected by hull-fixed accelerometers [*National Data Buoy Center (NDBC)*, 1996]. The frequency range of the waves sensible by the buoys is dictated by the dimensions of the buoys.

The wave spectra data typically range from 0.02 to 0.485 Hz. For linear waves, this corresponds to 0.0016 rad/m to 0.95 rad/m in wavenumber, or about 4 km to 6.64 m in wavelength.

From the data, it is seen that most wind speeds range from 5 to 15 m/s. The wind speeds are measured at a height of 5 m.

Most buoys acquire wave data for a duration of 20 min each hour, at 20 min. to 40 min. after the hour. These measurements are then averaged to derive the wave spectrum, which is reported at hourly intervals.

Not all measurements are taken continuously and simultaneously. A data product known as "continuous wind," however, is measured continuously, and is averaged every 10 min. The first continuous wind measurement of the hour starts at minute 0 and ends at minute 10.

Meteorological data such as air temperature and SST are 8 min averages, collected hourly from 42 to 50 min after the hour [*NDBC*, 2009b]. The air temperature is measured at a height of 4 m.

NDBC historical data were accessed from [*NDBC*, 2015]. We take the time of each measurement to be at the center of the averaging period. For example, a wind measurement averaged from 10 to 20 min after the hour is taken to be the wind speed at 15 min after the hour. Likewise, the wave measurements made between 20 and 40 min after the hour are taken to be the sea state at 30 min after the hour. (It should be noted, however, that the reported timestamps in NDBC data sets are not at the center but vary by the type of measurement [*NDBC*, 2012a]; care is taken to interpret the timestamps correctly.) To synchronize the wind and wave data, both data sets are interpolated to 5 min intervals. A spectrum-preserving sinc interpolator is used. For other meteorological data, only long-term averages are needed for our analysis and so no interpolation is necessary.

Due to vandalism and possibly other issues (e.g., recovery and redeployment) [*Teng et al*., 2010], the data sometime contain gaps. If the gap is less than 1.5 h, data are filled in by interpolation. Otherwise, the data series is broken into chunks for processing. This is of relevance because our analysis techniques (see sections 3.1 and 3.2) require a continuous series of data.

A list of buoys selected for use in this analysis, along with their relevant properties, can be found in Appendix A (Table A1). The distance to the nearest coast is obtained from *NASA's Ocean Biology Processing Group* [2009] data set. For bathymetry, the cell-registered version of ETOPO1 [*Amante and Eakins*, 2009] is used.

Stations with any of the following characteristics are excluded from the analysis:

1. Nonstandard wave acquisition times [*NDBC*, 2012b, 2002],
2. Anemometer not at the usual 5 m height, or the air temperature sensor not at the usual 4 m height [*NDBC*, 2009a],
3. Location with ocean depth less than 193 m (see section 2.2 for explanation), and
4. Location less than 10 km from the coast.

Older spectral data, which do not range from the typical 0.02 Hz to 0.485 Hz, are also excluded.

2.2. Computation of Mean Square Slope

Because the mss is a spatial property, the one-dimensional frequency spectrum measured by buoys first needs to be converted to a wavenumber spectrum. The linear dispersion relation in deep water is invoked to perform this conversion. To ensure that the deep water approximation holds, we exclude buoys in shallow coastal waters, in which the behavior of waves is significantly more complicated [*Donelan et al*., 2012]. To compute a depth threshold, we first note that the wind speeds measured by buoys rarely exceed 20 m/s. From the fully developed Elfouhaily spectrum [*Elfouhaily et al*., 1997] at 20 m/s, the dominant waves have a wavenumber of approximately 0.0163 rad/m, and this corresponds to a wavelength of about 386 m. Since the deep water approximation is generally valid at depths of greater than $1/2$ the wavelength, the depth threshold is set at 193 m.

The low pass filtered mss (LPmss) is then computed as

$$LP_{mss}(k_x) \triangleq \int_0^{k_x} k^2 S(k) dk, \tag{1}$$

where $S(k)$ is the wavenumber elevation spectrum with SI units of m^3, k is the wavenumber, and k_x is the upper limit of integration. As noted above, for the 3 m discus buoys, the upper wavenumber of the waves the buoys are capable of sensing is about 1 rad/m. In practice, there is also a lower bound. This lower bound is small enough to be not of significance, because not only is there little wave energy in the longer wavelengths, the mss statistic also emphasizes the higher wavenumber portions of the wave spectrum.

For short waves, it is known that the current or longwave-induced Doppler shift may be a significant source of error in blind applications of the above conversion procedure. The Doppler frequency shift is equal to $\vec{k} \cdot \vec{c}$, where $\vec{k}$ is the vector wavenumber and $\vec{c}$ is the vector current velocity. The wavelengths measured by discus buoys are comparatively long, so, as will be discussed sections 7 and 8, a bound can only be computed for certain microwave sensing methods (L-band and above, for instance). These relatively long wavelengths fortuitously imply that the Doppler shift can be ignored given the typical magnitudes of current velocities [*Hwang*, 2005b].

2.3. Separation Frequency and Swell

For this study, wind seas are of exclusive interest. Field data inevitably include both swells and wind seas. Winds in nature are also never truly constant nor steady in time or space, so the division between wind seas and swell is somewhat artificial. A common method used to separate swell and wind seas for a 1-D spectrum involves the designation of a "separation frequency," above which the waves are classified as wind seas; the rest are taken to be swell [e.g., *Hwang et al*., 2012]. In this study, no separation frequency is used for the following reasons. First, the division between wind seas and swell is seldom clear-cut. As wind seas become more mature, the peak frequency downshifts and may occupy the same frequency band as swell, in which case the application of a separation frequency is no longer justified. Second, the mss is dependent on the wavenumber limits of integration. Even if the region of overlap between wind sea and swell wavenumber is small, if the separation frequency is changed at each instant in time, errors in the estimation of the separation frequency and in their changes could introduce artificial signals in the mss that affect the correlation between wind and waves. Introducing a constant separation frequency would be equivalent to considering only a bandpass filtered version of the mss, which has been carried out in [*Chen et al*., 2012]. (It should be noted that the results in *Chen et al*. [2012] overestimate the lag time by approximately 25 min due to an erroneous interpretation of the wind and wave acquisition times.)

Swell is, by definition, uncorrelated with the local *wind*. Swell may well be correlated (albeit indirectly) with the response of the *waves*, however. The level of swell, as well as its direction, is expected to be highly correlated with location, which in turn is related to the fetch, and, as shown in section 5, fetch has a strong effect on the evolution of the wind sea. But this relationship is correlative only – swell does not *cause* the response time to shift, because it has zero correlation with temporal changes in the wind speed. Thus, whether swell is removed in processing or not is immaterial to the response time itself. In particular, given our method for determining response time (discussed in the next section), the presence of swell, or lack thereof, is only expected to shift the noise floor, but not the response time statistic itself.

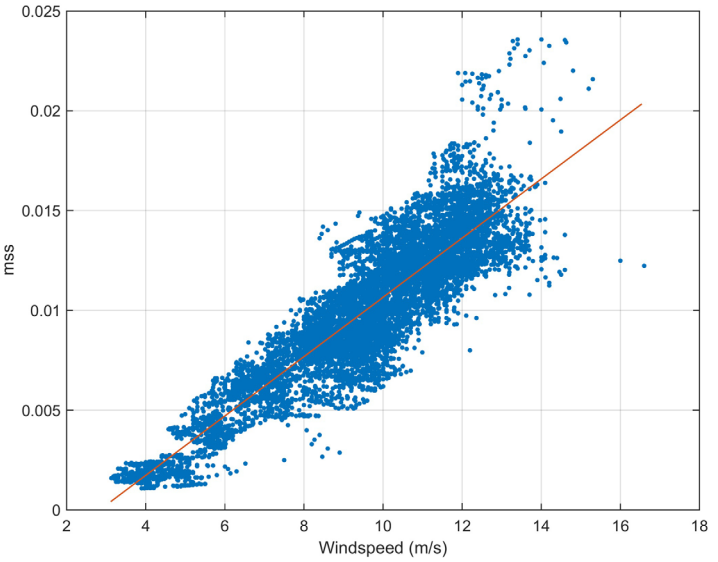


Figure 1. Scatter plot of the wind speed and mss measurements made by Station 42058 from 1 to 31 January 2009, with no lag time applied. The quadratic fit is shown in red.

3. Response Time Analysis

In deep water, the action balance of waves dictates that the growth of waves is dominated by three source terms: input due to wind forcing, dissipation due to breaking, and nonlinear quadruplet wave-wave interactions. When there is a net energy input, the waves grow continuously, and the rate of growth decreases over time. Whether there exists an asymptotic limit, the so-called "fully developed" condition, remains an open question [*Hwang and Wang*, 2004a]. Drawing from the theory of duration-limited and fetch-limited growth of dimensionless energy and frequency, we are led to propose that the growth of mss, a nondimensional quantity, can be expressed as a function of dimensionless duration and dimensionless fetch:

$$mss = F(t^*, x^*) \tag{2}$$

where $t^* = tg/U$ is the dimensionless duration and $x^* = xg/U^2$ is dimensionless fetch, both scaled by a wind speed U at some arbitrary height. t and x are the corresponding dimensional quantities, and g denotes the gravitational acceleration.

In the following analysis, instead of attempting to derive the growth functions themselves, we restrict our analysis to the determination of a single characteristic response time. Because the winds are nonsteady, there is no obvious choice for the wind speed scaling. We therefore focus on the determination of a dimensional response time in this study, and reserve consideration of a nondimensional growth function for future work.

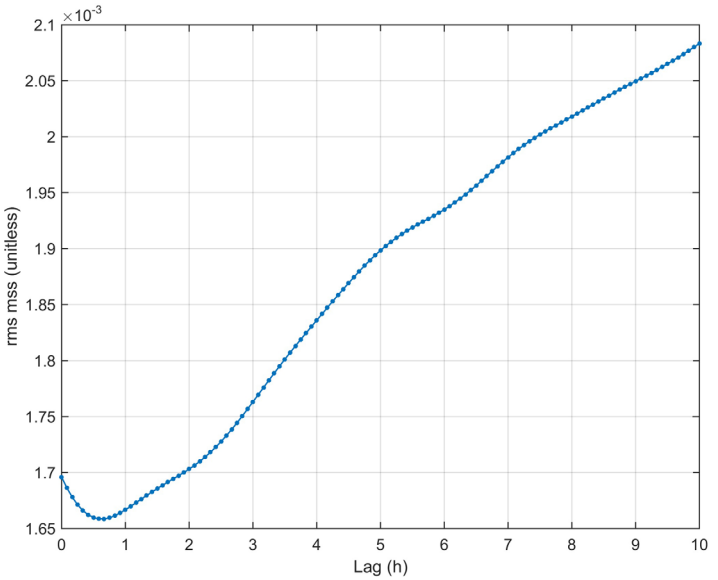


Figure 2. Residual RMS difference versus lag time, for Station 42058 from 1 to 31 January 2009.

3.1. Response Time Methodology

Chen et al. [2012] previously presented a definition of response time based on the lag-correlator. The lag-correlation between two continuous-time signals $r(\tau)$ and $s(\tau)$ is defined as the convolution given by

$$\psi_{rs}(t) \triangleq \lim_{T\to\infty} \int_{-T}^{T} r(\tau'+t)s(\tau')d\tau'. \tag{3}$$

The response time was then defined as the time lag, t, at which the lag correlation is maximized. We propose here an alternative definition for response time that is found to

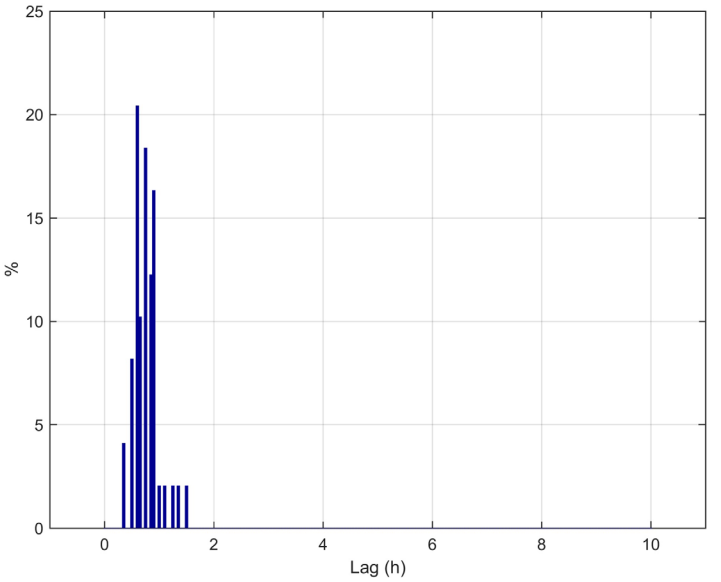


Figure 3. Histogram of response times derived from consecutive 30 day measurements of Station 42058 over 11 years (2004–2014, inclusive). The response times are found by minimizing the residual RMS difference.

be much less susceptible to noise in the wind and wave data. The alternative procedure follows these steps:

1. Start with a time series of wind speed and mss data, $U(t)$ and $mss(t)$, for a given buoy.
2. Form a population of sample pairs, $\{U(t), mss(t-\tau)\}$, where τ is a (variable) time lag.
3. Perform a least-squares, second order polynomial fit between $U(t)$ and $mss(t-\tau)$. Note the residual RMS difference in the fit.
4. Vary the time lag, τ, and find the lag which minimizes the residual RMS difference. This lag is defined as the response time.

An example of this procedure is presented in the section 3.2. We then use the procedure to derive a stable, long term response time, and discuss general characteristics applicable to all cases. In this paper, we will refer to this method as the RMS minimizer, in contrast to the lag-correlator.

3.2. Example of Response Time Determination and Discussion

We consider here the continuous 30 day wind and mss measurements made by Station 42058 from 1 to 31 January 2009. A scatter plot of the wind speed and mss measurements with no lag time applied is shown in Figure 1.

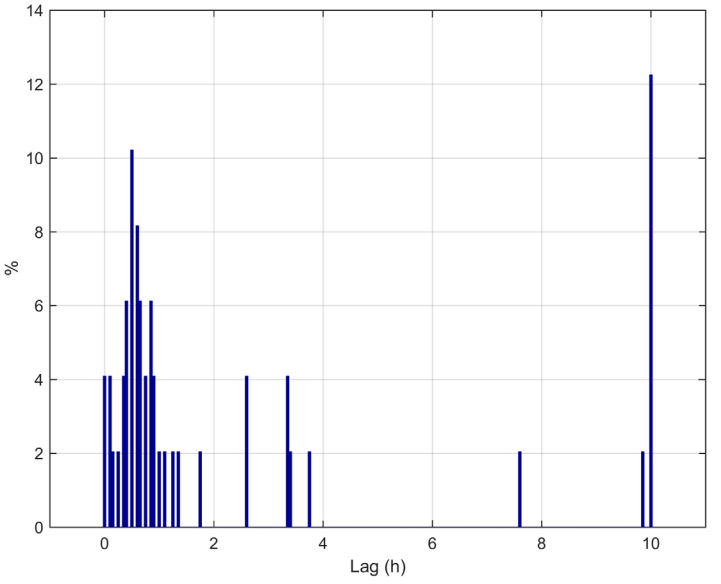


Figure 4. Histogram of lag-correlation response times found derived from consecutive 30 day measurements of Station 42058 over 11 years. These response times are found to be less stable than the ones derived by minimizing the RMS residual, so they are not used in this paper.

The scatter could be due to swell, duration, and other factors considered in the following sections. In addition, scatter is also contributed by averaging and interpolation––we recall the waves are 1 h averages while the winds are 10 min averages. We see, later, however, that by leveraging the data collected over 11 years, we can derive with some confidence a response time better than 1 h in resolution.

We note that the swell contributes a positive bias to the wind sea mss; the mss in the scatter plot is not just due to wind waves. However, as noted, the swell is uncorrelated with wind speed and changes in wind speed. Therefore, it does not impact the derived response time. However, note that inclusion of the swell

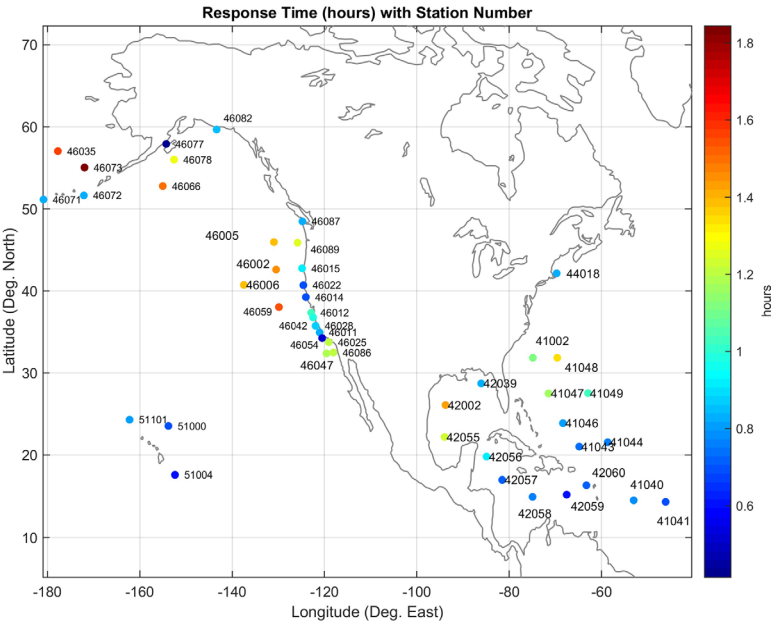


Figure 5. Response times of the 46 buoy stations under study. Data used to generate this plot can be found in Dataset S1, as part of the Supporting Information associated with this paper.

mss is desirable if we are trying to derive a geophysical model function that relates wind speed to the remotely sensed mss observable, because the mss observable also includes swell contributions.

A least-squares, second order polynomial fit is applied to the data shown in Figure 1, and the residual RMS difference is noted. This is then repeated using time lags of between 0 and 10 h. The resulting residual difference versus lag time is shown in Figure 2.

The time lag at which the residual RMS difference is minimized is found to be 40 min (∼0.7 h). This, then, is the response time of the mss to the local wind speed for this 30 day data set.

It should be noted that the above procedure needs to be applied to continuous, gap-free wind and wave signals to ensure the proper time match-up of lagged waves and wind. We apply the above method to all continuous 30 day signals over the full 11 years of data for the same buoy. A histogram of the resulting response times for Buoy Station 42058 is shown in Figure 3.

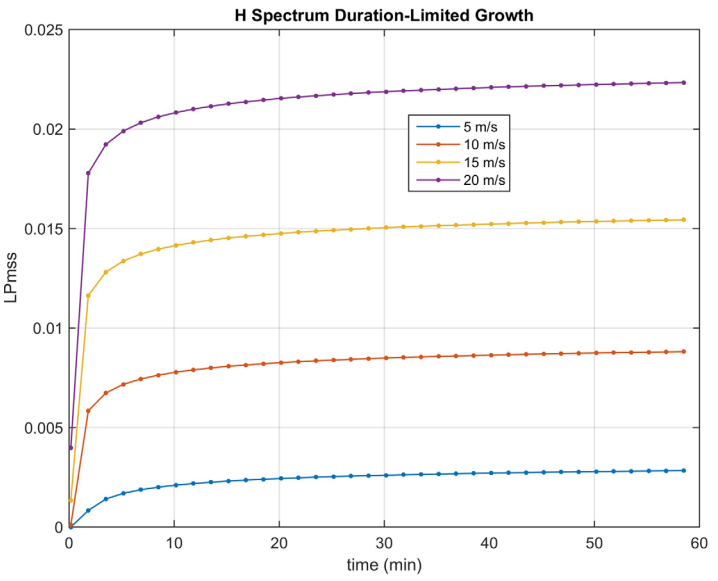


Figure 6. Duration-limited growth of LPmss, as predicted by the wave-age dependent H spectrum. Note the unit for time on the abscissa is minutes.

Note that, while there is some spread in the derived response time over the 11 years, the distribution is not uniform but rather highly localized. The mean value of the response time is found to be ∼0.8 h (45 min). *This value is considered as our best estimate of the response time for Station 42058.*

For comparison, we apply the lag-correlator technique used in *Chen et al.* [2012] to the same data set in 30 day segments.

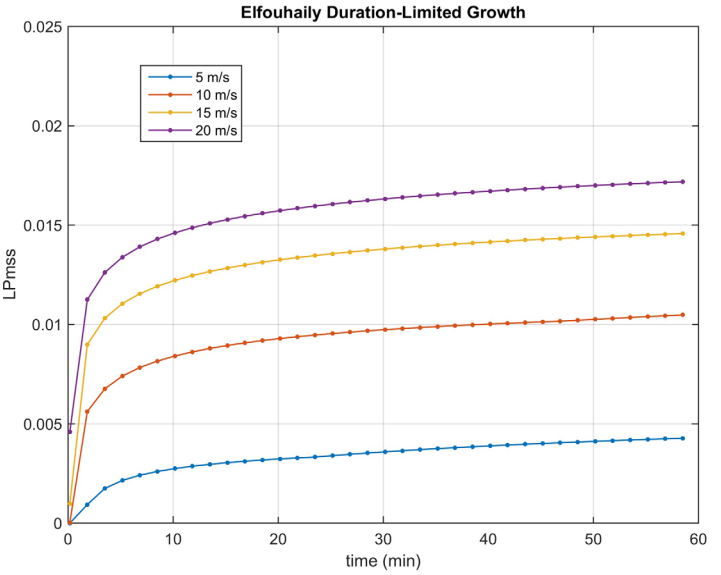


Figure 7. Duration-limited growth of LPmss, as predicted by the wave-age dependent Elfouhaily spectrum. Note the unit for time on the abscissa is minutes.

Figure 4 shows the histogram of response times produced using its procedure.

The lag-correlator method is seen to be less stable, and sometimes misidentifies the wind wave response resulting in a more than 10 h lag. Response times greater than 10 h are not believed to be physically reasonable – when the signal lengths are increased, these anomalously long lags are no longer seen. Because of this, the lag-correlator is not used in this study.

3.3. Results for All Buoys

Forty-six NDBC buoys were found to satisfy the criteria specified in section 2.1. We apply the RMS minimization procedure to all 46 buoys, with 11 years of data, to obtain response times for each location. Data in all field conditions are used. Figure 5 shows a map of the response time derived at each buoy location.

The response times are seen to vary between 0.4 and 1.8 h. It is also seen that, in general, stations with a close proximity to one another have similar response times, likely because they are subjected to the same environmental conditions. In sections 4–6, we investigate the dependencies of these response times on environmental factors.

3.4. Comparisons to Models of Duration-Limited Wave Growth

Hwang et al. [2013], *Hwang and Fois* [2015], and *Elfouhaily et al.* [1997] designed models of wave spectra that depend on wind speed and wave age. By using the second-order duration-limited growth functions from [*Hwang and Wang*, 2004a, 2005], the wave age can be computed knowing the duration and wind speed. The wave age and wind speed can then be used with the wave spectrum models to compute an LPmss bounded above by 1 rad/m (as measured by the buoys). The duration-limited growth of LPmss predicted by the two wave spectra are shown in Figures 6 and 7.

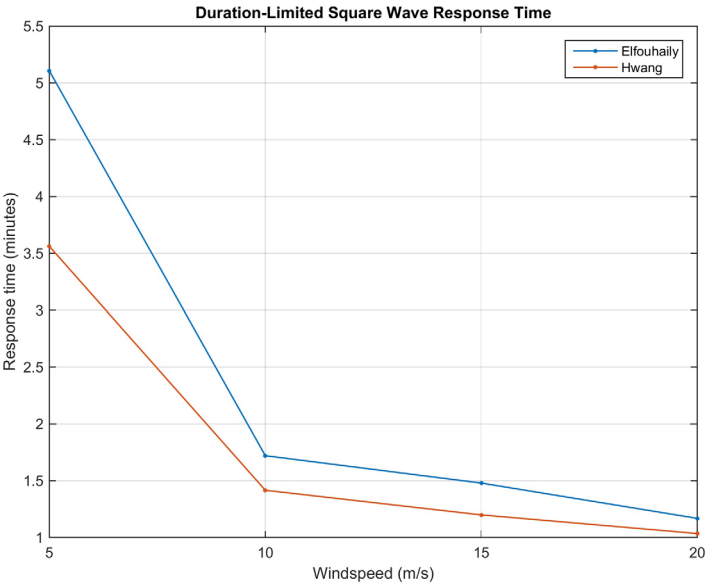


Figure 8. Response time versus U10 magnitude, as predicted by the H and Elfouhaily spectra. Note the unit of the ordinate is minutes.

Duration-limited growth assumes a wind speed step function waveform starting at 0 m/s up to the scaling wind speed magnitude (varied from 5 to 20 m/s in Figures 6 and 7). As mentioned in section 1, duration-limited growth implies large fetch. In reality, wind speed

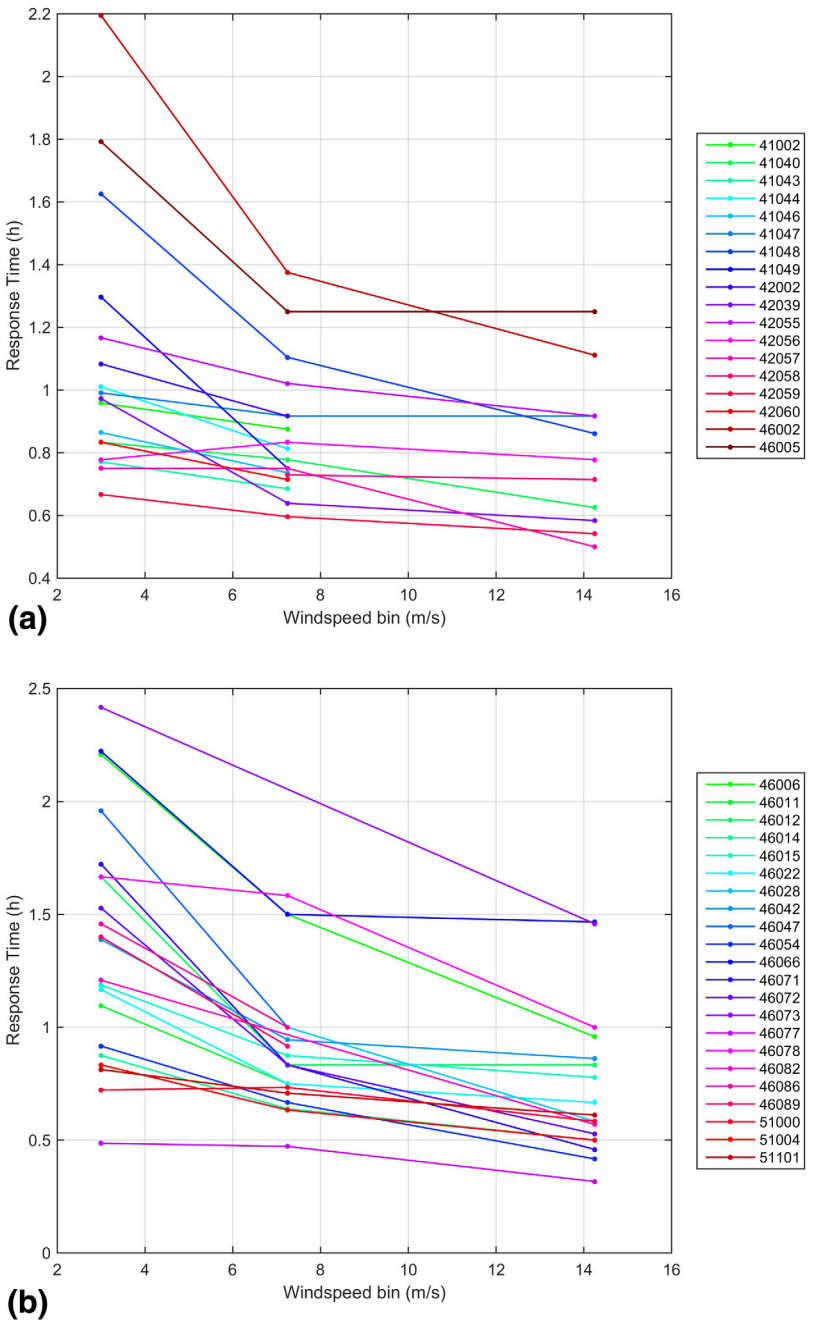


Figure 9. Response time dependency on wind speed magnitude. Data used to generate this plot can be found in Data Set S1, as part of the supporting information associated with this paper.

fluctuations are not step functions starting from calm conditions, the fetch is finite, and the correlation of wind and waves incorporates wave growth as well as wave decay.

However, the response time (as defined in section 3.1) of wave growth in ideal duration-limited conditions can be derived from the results in Figures 6 and 7. An approximate estimate of the response time corresponds to the time the duration-limited LPmss grows to 50% of its final, steady state value (assuming one exists). Had the wave response been a ramp function, this estimate obtained with this method would be perfect. The response times derived thus are shown as a function of wind speed in Figure 8.

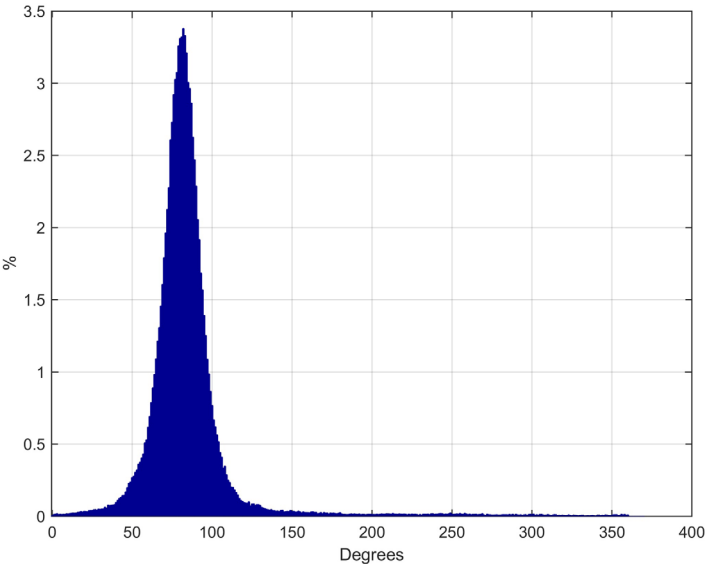


Figure 10. Wind direction histogram of 42058 over 11 years. The wind direction is clockwise from the North, and indicates the direction the wind is coming from. It is seen that the dominant wind direction is from East to West for Station 42058.

The response times corresponding to wave growth, as predicted by the two models, are seen to be significantly lower than the empirical results found from the NDBC buoy data. This could be due to a much slower wave decay rate than growth rate, or the overestimation of the wave growth rate in the models. Further study, perhaps with data collected in carefully controlled conditions, is needed to resolve this question.

4. Dependence of Response Time on Wind Speed

The analysis based on wave spectra models, as illustrated in Figure 8, predicts that the response time decreases as wind speed increases. To assess whether this behavior is also exhibited by the NDBC buoy data, we apply the same RMS minimization procedure discussed in sections 3.1 and 3.2 to the wind speed and LPmss data of each buoy, except now we bin the data according to wind speed and consider the data in each bin separately. The response times identified for each bin are then averaged. We consider 3 wind speed bins: 0 – 6 m/s, 6 – 8.5 m/s, and 8.5 – 20 m/s. The binning was made nonuniform because most data fall between 5 and 15 m/s; even so, there is insufficient data for some bins for some buoys, in which case a response time cannot be determined reliably for that case.

Due to the number of buoys, we present the results in two separate plots in Figure 9 to avoid clutter:

In almost all cases, a monotonically decreasing response time for increasing wind speed is evident, in agreement with the models.

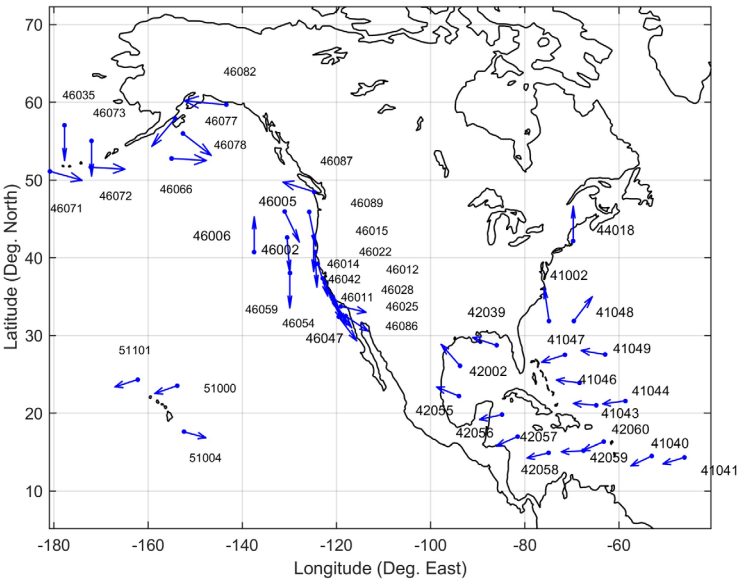


Figure 11. Dominant wind directions for the 46 buoys under study. The arrows point downwind. Data used to generate this plot can be found in Data Set S1, as part of the supporting information associated with this paper.

5. Dependence of Response Time on Fetch

Fetch is often difficult to quantify. In this section, fetch is not explicitly calculated. We are able to make inferences of the relative magnitudes of fetch, however, by examining the dominant wind direction in some locations.

The histogram wind direction for all 11 years of data is presented in Figure 10 for Station 42058 as an example. Station 42058 is located in the middle of the Caribbean Sea with a nominal position of 14°55′23″ N, 74°55′4″ W.

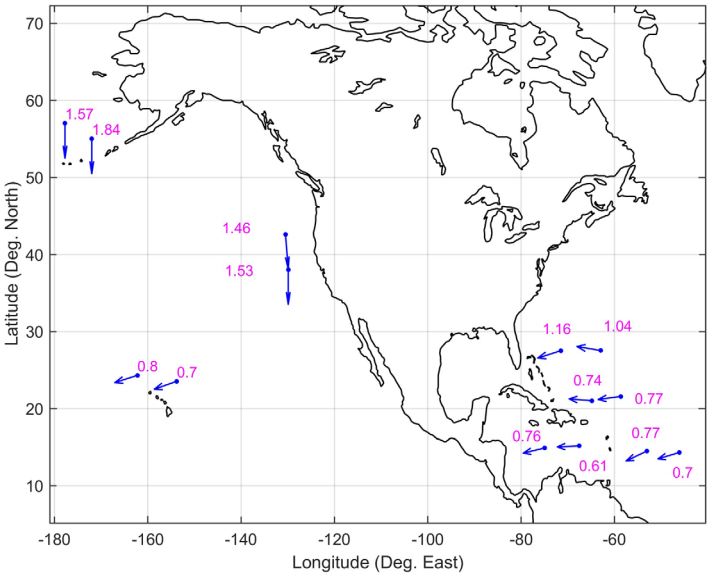


Figure 12. The arrows point in the direction the wind is blowing toward. Numeric labels correspond to response time in hours. Stations 41043 (downwind) and 41044 (upwind) are circled in red; their response times in the context of fetch is discussed in the text.

The wind direction convention is clockwise from the North, and indicates where the wind is coming from.

We define the dominant wind direction to be the direction where the distribution is maximum. The maximum is used instead of the average, because the wind direction distribution may be multimodal.

In Figure 11, we plot the dominant wind directions for all 46 buoys. The arrow points downwind (in the direction of air flow).

We then choose suitable locations for fetch studies. The locations should be close in proximity with approximately the same wind direction, because it is desirable that winds do not change appreciably over these distances. Only locations far from land are considered to avoid coastal wave processes such as reflection and bottom refraction. The selected stations, along with the response times, are shown in Figure 12.

We see that in all cases but one, the downwind location, with larger fetch, has a longer response time. The one exception is circled in red. This is possibly because the downwind station, 41043, has a slightly higher average wind speed (0.3 m/s) than the upwind station. Section 6 indicates that the atmospheric stratification is less stable on average at 41043 than 41044, which may also contribute to the lower response time of 41043.

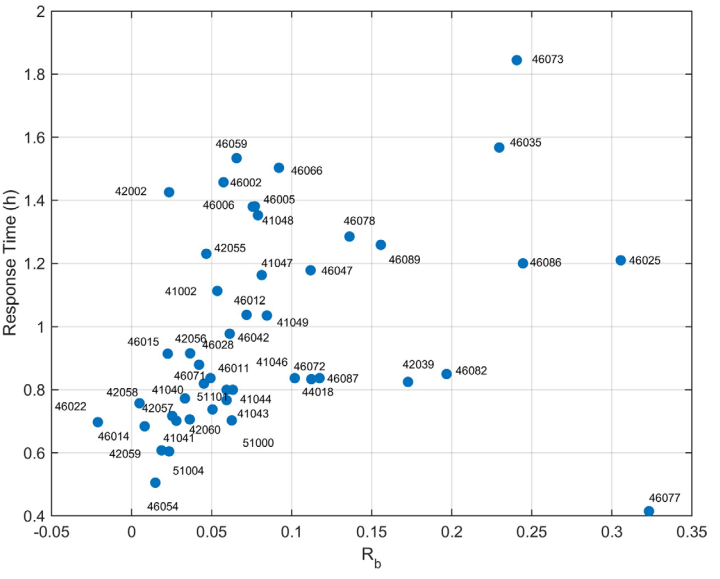


Figure 13. Wave response time versus the Bulk Richardson Number. A positive correlation is seen, indicating lower atmospheric stability corresponds to a faster response. Data used to generate this plot can be found in Data Set S1, as part of the supporting information associated with this paper.

6. Dependence of Response Time on Atmospheric Stability

Kahma et al. [1992] analyzed six well-known fetch-limited data sets available at the time in an attempt to reconcile the differences in wave growth. They derived the fetch-limited growth relations separately for unstable and stable conditions, and noted that unstable stratification enhanced wave growth, even when using friction velocity as the scaling wind speed. *Young et al.* [1998] analyzed data from the Lake George experiment, which is documented in [*Young and Verhagen*, 1996], using the Bulk Richardson Number to characterize atmospheric stability. It is defined as

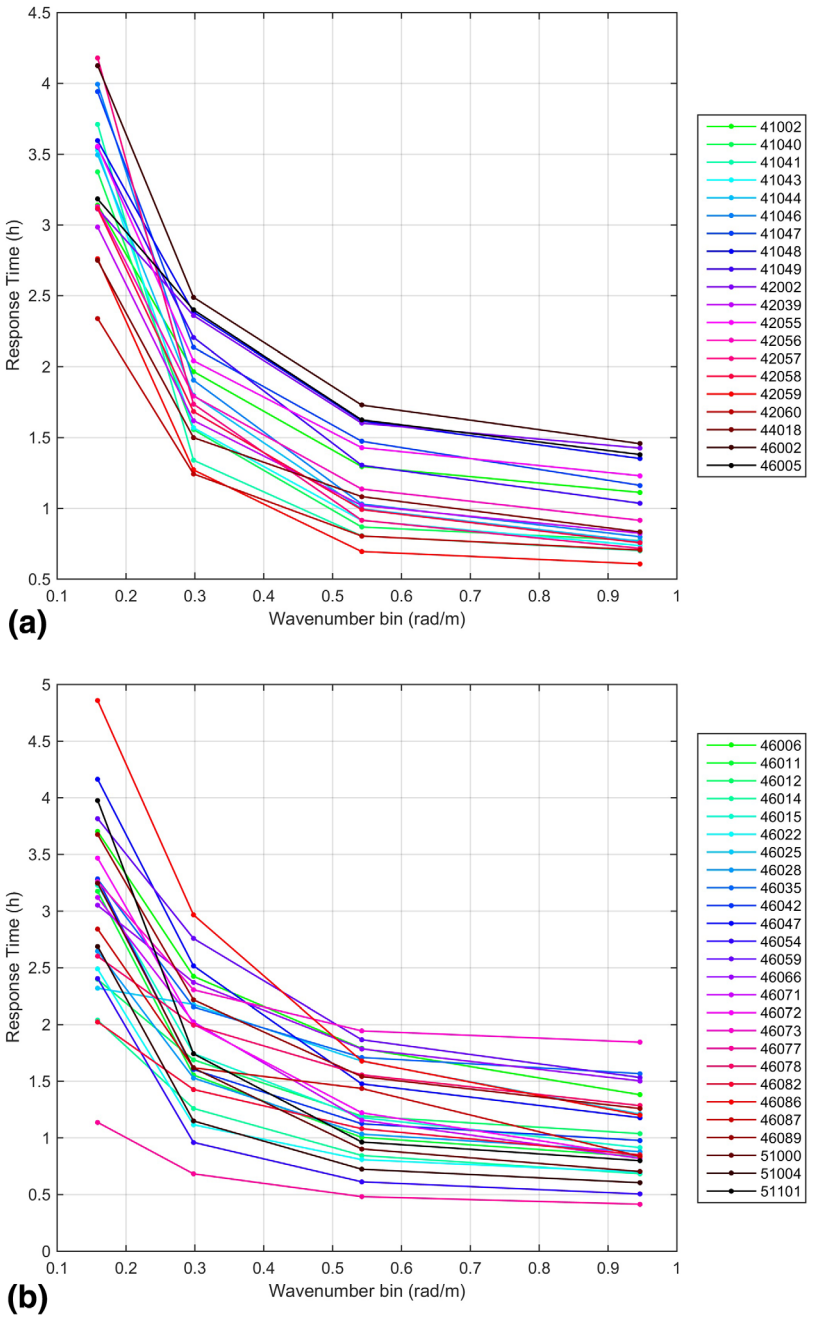


Figure 14. Response time dependency on upper limit of integration of LPmss. Data used to generate this plot can be found in Data Set S1, as part of the supporting information associated with this paper.

$$R_b = \frac{g(T_a - SST)}{z_t T_a (U/z)^2}, \tag{4}$$

where SST is the sea-surface temperature, T_a is the air temperature at height z_t, and U is the wind speed at height z. Thus, negative values are indicative of unstable stratification while positive values represent stable conditions. In addition to other findings, they concluded that wave growth is more pronounced (as a function of fetch) in unstable conditions, in agreement with *Kahma et al.* [1992]. Since duration-limited growth can be related to the fetch-limited growth using the space-time conversion relations [*Hwang and Wang*, 2004a], we expect that waves grow more rapidly as a function of time in duration-limited cases as well. This implies a shorter response time in less stable conditions, which we now verify.

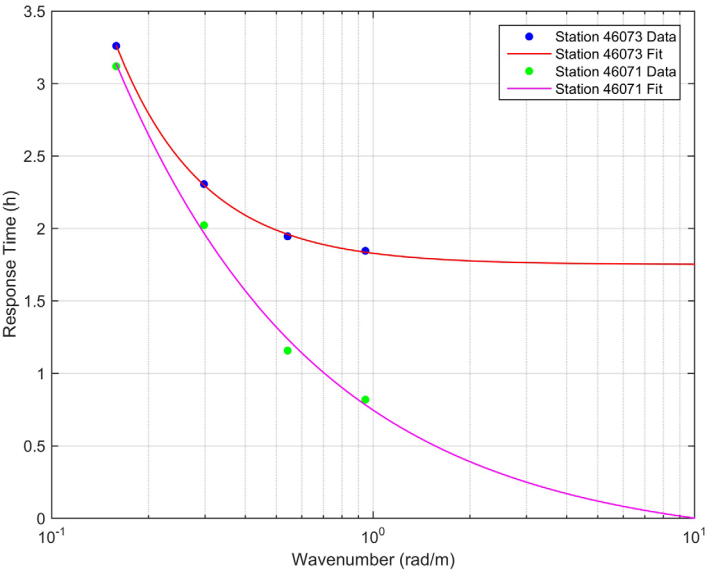


Figure 15. Power function (equation (5)) fittings of the wavenumber dependency of response time, for the two station with extremal response times at L-band. Note the logarithmic scale on the abscissa.

In the following analysis, we also employ the Bulk Richardson Number as a measure of stability, using the averaged 5 m height wind speed for scaling. Averaged T_a and *SST* values are used in equation (4) to compute an R_b for each station, and this is then plotted against the response time in Figure 13.

A positive correlation is seen, with lower atmospheric stability being associated with a shorter response time, in agreement with previous empirical studies. Our results, therefore, support the idea [*Young*, 1998] that wave growth similarity theory should be augmented with a dimensionless group characterizing atmospheric stability, in addition to dependencies on dimensionless fetch and duration. The apparent outlier in Figure 13, Station 46077, is located just south of Alaska and north of an island. This station likely experiences short fetch wave conditions, and this may contribute to its short response time.

7. Dependence of Response Time on Wavelength and Implications for L-Band Remote Sensing

We now investigate the behavior of the response time as the upper limit of integration in equation (1) is varied. Note that, instead of analyzing the bandpass mss studied previously by *Chen et al*. [2012], we study the LPmss, which is of interest to bistatic sensors and radar altimeters. We choose 4 upper limits, and they are chosen so that the cumulative distribution function (CDF) of LPmss as a function of wavelength attains 25%, 50%, 75% and 100% respectively for the 4 LPmss'es. (The CDF is computed using the Elfouhaily wave spectrum, which is very similar to the CDF derived from the H spectrum.)

Similar to the method used to analyze the wind speed dependency, we average the response times for each LPmss and each buoy for 11 years. The results are presented in the two plots of Figure 14.

The response time is seen to decrease monotonically as the upper wavenumber is increased, for almost all of the buoys under study. This is consistent with the present understanding on wind-wave growth: shorter waves become well-developed first, when the energy they possess saturates. At this point, further energy input from wind is either dissipated by breaking or transferred to longer waves by nonlinear interactions.

Spaceborne L-band bistatic remote sensing of ocean surface wind speed has recently been proposed by *Ruf et al*. [2012]. In the rest of this section, we obtain rough estimates of the response times at L-band by extrapolation. It was found that power functions of the form of equation (5) fit the data well for almost all of the buoys under consideration.

Table 1. Parameters of the Fitted Power Function (equation (5)) for the Stations With Extremal Response Times

	a	*b*	*c*
Station 46073 (Max. Response Time)	0.07758	−1.614	1.751
Station 46071 (Min. Response Time)	0.996	−0.8508	0.1071

$$t(k) = ak^b + c \tag{5}$$

Functional fittings are performed for all 46 stations, and the fitting function is then used to extrapolate to a response time at L-band (10 rad/m). The fitting function for one station resulted in a nonphysical negative response time at L-band, which we

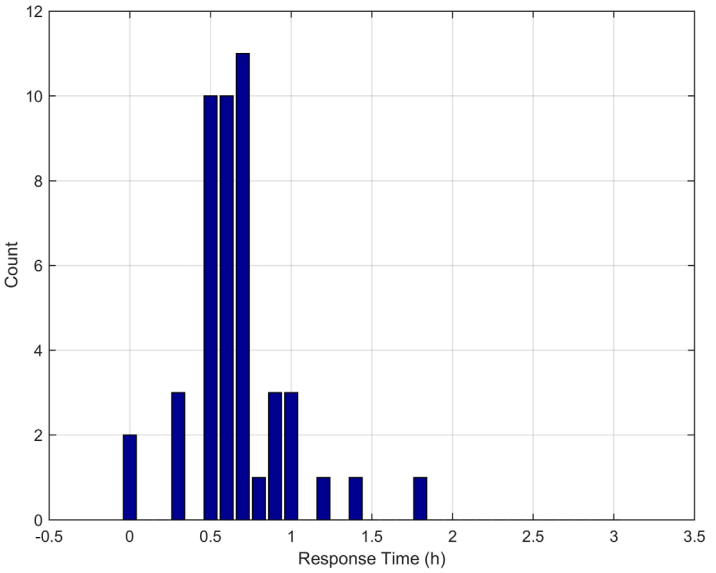


Figure 16. Histogram of the estimated L-band response times for the 46 buoys under study.

take to be 0 for the statistics presented in the rest of this section. The function fittings for two stations are shown in Figure 15—these being the ones with the maximum and minimum (physical) response times. The parameters of the fitting functions for these two stations are listed in Table 1.

A histogram of the L-band response times derived for the 46 buoys is shown in Figure 16. It is seen that over 93% of the L-band response times fall between 0.3 and 1.4 h, with a mean of 0.66 h.

Weissman et al. [1996] analyzed the spectral correlation of wind and waves using data from an L-band scatterometer and a sonic anemometer. The radar data consisted of about 4 days of data in records of about 5 min long, which confined the applicability of their results to fluctuations on the order of 0.01 Hz and higher. The low coherence they found at L-band implies that if an L-band response time can be identified, it would be greater than timescales of 100 seconds. Our results are, therefore, in general agreement with this conclusion.

It should be noted that the response time extrapolation to L-band is speculative, and measurements of mss at these wavelengths, in a variety of conditions, would be needed validate this result.

8. Concluding Remarks

In this work, we analyzed collocated wind and wave data measured by 64 moored discus buoys over 11 years. We found the response times of mss to wind forcing for each buoy to be reasonably stable, and all response times are bounded between 0.4 and 1.8 h. We also find that the mss response time is dependent on wind speed magnitude, fetch, atmospheric stability, and wavelength. The response times are, however, much greater than what current models of wave age dependent wave spectra predict. This may be due to effects of wave decay or inaccurate wave age dependency in the models.

Our results would be directly relevant to HF and VHF remote sensing of the ocean. They can also serve as bounds for L-band bistatic remote sensing. The Cyclone Navigation Satellite System (CYGNSS) is a spaceborne L-band bistatic mission to be launched in late 2016 [*Ruf et al.*, 2016]. Integrations of the H spectrum reveal for wind speeds ranging from 5 to 15 m/s, which constitutes most of the data collected by NDBC buoys, 50% of the LPmss sensitivity to wind is due to waves 6.6 m and longer (the NDBC buoy wavelength range). This percentage is very sensitive to wind speed, and becomes higher as the wind speed increases.

For CYGNSS's incidence angle, the upper wavenumber limit sensed is about 10 rad/m. We saw in section 7 that the extrapolated L-band response exhibits a rather large variability about a mean of 0.66 h. We noted that our results are in keeping with previous observations by *Weissman et al.* [1996]. *Chen et al.* [2012] showed that response times of bandpass filtered mss also decreases monotonically with increasing wavenumber, so our results are also applicable to L-band scatterometers like SMAP [*Entekhabi et al.*, 2010]. Furthermore, this study indicates that ancillary data such SST and air temperature could be beneficial in improving the accuracy of the wind retrievals.

Finally, we note that the data used in this analysis are limited in wavelengths sensed by the buoys (on the shorter end). In-situ measurements of short, intermediate-scale waves can be quite challenging [Hwang, 2005b]. Remotely sensed data, like those to be provided by CYGNSS, coupled with collocated in situ wind measurements, will likely be invaluable for advancing our understanding of this topic.

Appendix A

Data presented in Table A1 can be found in Data Set S1, as part of the supporting information associated with this paper.

Table A1. Buoy Stations and Their Properties

Station Number	Latitude (Deg. North)	Longitude (Deg. East)	Ocean Depth (m)	Distance to Coast (km)	Average Wind Speed (m/s)	Wind "From" Direction (Deg. Clockwise from North)	Average Air Temperature (Celsius)	Average SST (Celsius)
41002	31.86	−74.84	4091	342	6.89	169	23.40	22.52
41040	14.52	−53.02	4898	708	6.98	74	27.74	26.99
41041	14.33	−46.08	3587	1233	7.1	80	26.82	26.18
41043	21.02	−64.85	5286	256	6.26	94	27.32	26.44
41044	21.58	−58.63	5418	543	6.13	86	27.07	26.13
41046	23.89	−68.37	5570	386	6.07	96	27.01	26.02
41047	27.52	−71.48	5291	482	6.1	79	25.85	24.57
41048	31.87	−69.57	5358	447	6.82	225	23.93	22.51
41049	27.54	−62.95	5433	553	5.65	98	25.66	24.55
42002	26.09	−93.76	3063	341	6.44	129	25.63	25.29
42039	28.74	−86.01	293	122	5.63	104	24.86	22.58
42055	22.2	−94	3637	304	6.47	106	27.33	26.48
42056	19.8	−84.86	4569	213	6.6	83	28.38	27.40
42057	17	−81.5	423	225	6.71	75	28.35	27.83
42058	14.92	−74.92	4158	356	8.7	82	27.98	27.81
42059	15.18	−67.56	4780	307	7.32	89	28.23	27.76
42060	16.33	−63.24	1572	83	6.67	76	28.22	27.51
44018	42.14	−69.71	225	31	6.4	180	10.57	9.92
46002	42.61	−130.49	3454	487	7.08	354	13.67	13.07
46005	45.96	−131	2748	504	7.38	329	13.30	12.46
46006	40.75	−137.46	4235	1096	7.3	180	14.86	14.00
46011	34.96	−121.02	454	30	5.59	322	13.51	13.16
46012	37.36	−122.88	237	35	5.88	325	12.87	12.36
46014	39.24	−123.97	398	16	5.93	337	11.71	11.53
46015	42.76	−124.83	456	22	6.94	360	11.41	11.21
46022	40.72	−124.53	357	22	5.88	356	11.76	11.90
46025	33.75	−119.05	887	28	3.61	278	16.93	15.87
46028	35.75	−121.88	1138	40	6.74	325	13.76	13.31
46035	57.03	−177.74	3706	444	9.04	0	4.36	3.29
46042	36.79	−122.45	2001	35	5.98	325	13.28	12.80
46047	32.4	−119.54	1390	90	6.28	312	16.05	15.01
46054	34.26	−120.48	488	20	7.28	315	13.71	13.55
46059	38.05	−129.9	4570	538	7.02	360	15.11	14.26
46066	52.79	−155.05	4445	334	8.06	270	7.47	6.74
46071	51.14	179.12	1313	25	7.59	282	6.10	5.84
46072	51.66	−172.16	3583	71	8.03	270	5.99	5.44
46073	55.03	−172	3474	224	9	0	5.68	4.10
46077	57.89	−154.29	206	20	7.19	40	7.03	5.12
46078	55.99	−152.64	4357	100	7.96	306	7.98	6.82
46082	59.67	−143.39	302	44	6.74	101	8.65	7.40
46086	32.49	−118.03	1844	47	4.31	294	17.40	16.14
46087	48.49	−124.73	259	11	5.09	109	10.02	9.51
46089	45.89	−125.82	2401	141	6.34	346	12.72	11.71
51000	23.54	−153.81	4856	377	6.53	78	23.47	22.35
51004	17.6	−152.4	5098	330	7.55	279	25.35	24.81
51101	24.32	−162.23	4839	145	6.69	79	24.84	23.78

Acknowledgments
The authors would like to thank Richard Bouchard and John Tancredi of NDBC for their assistance in the interpretation of NDBC data and Paul Hwang for providing the code for the H spectrum. Mounir Adjrad, Dallas Masters, Valery Zavorotny, Mark Donelan, and Bill Plant are also acknowledged for their input. Data is furnished by NDBC [*NDBC*, 2015]. The work reported here was supported, in part, by the NASA Earth and Space Science Fellowship (NESSF) Program under grant NNX13AN77H and the NASA Science Mission Directorate under contract NNL13AQ00C.

References

Amante, C., and B. W. Eakins (2009), ETOPO1 1 arc-minute global relief model: Procedures, data sources and analysis, *NOAA Tech. Memo. NESDIS NGDC-24*, Natl. Geophys. Data Cent., NOAA, doi:10.7289/V5C8276M.

Chen, D. D., S. Gleason, C. Ruf, and M. Adjrad (2012), Spectral dependence of the response time of sea state to local wind forcing, in *2012 IEEE International Geoscience and Remote Sensing Symposium (IGARSS)*, IEEE, pp. 3776–3779, doi:10.1109/IGARSS.2012.6350495.

Cox, C. S., and W. Munk (1954), Statistics of the sea surface derived from sun glitter, *J. Mar. Res.*, *13*, 198–227.

Donelan, M. A., M. Curcic, S. S. Chen, and A. K. Magnusson (2012), Modeling waves and wind stress, *J. Geophys. Res.*, *117*, C00J23, doi:10.1029/2011JC007787.

Elfouhaily, T., B. Chapron, K. Katsaros, and D. Vandemark (1997), A unified directional spectrum for long and short wind-driven waves, *J. Geophys. Res.*, *102*, 15,781–15,796.

Entekhabi, D., et al. (2010), The Soil Moisture Active Passive (SMAP) Mission, *Proc. IEEE*, *98*(5), 704–716, doi:10.1109/JPROC.2010.2043918.

Hasselmann, K., et al. (1973), Measurements of wind-wave growth and swell decay during the Joint North Sea Wave Project (JONSWAP), *Dtsch. Hydrogh. Z.*, *8*(12), suppl. A, 95.

Hwang, P. A. (2005), Wave number spectrum and mean square slope of intermediate-scale ocean surface waves, *J. Geophys. Res.*, *110*, C10029, doi:10.1029/2005JC003002.

Hwang, P. A., and F. Fois (2015), Surface roughness and breaking wave properties retrieved from polarimetric microwave radar backscattering, *J. Geophys. Res. Oceans*, *120*, 3640–3657, doi:10.1002/2015JC010782.

Hwang, P. A., and D. W. Wang (2004a), Field measurements of duration-limited growth of wind-generated ocean surface waves at young stage of development, *J. Phys. Oceanogr.*, *34*, 2316–2326, doi:10.1175/1520-0485(2004)034<2316:FMODGO>2.0.CO;2.

Hwang, P. A., and D. W. Wang (2004b), An empirical investigation of source term balance of small scale surface waves, *Geophys. Res. Lett.*, *31*, L15301, doi:10.1029/2004GL020080.

Hwang, P. A., and D. W. Wang (2005), CORRIGENDUM, *J. Phys. Oceanogr.*, *35*, 268–270, doi:10.1175/JPO-2731.1.

Hwang, P. A., F. J. Ocampo-Torres, and H. García-Nava (2012), Wind sea and swell separation of 1D wave spectrum by a spectrum integration method, *J. Atmos. Oceanic Technol.*, *29*, 116–128, doi:10.1175/JTECH-D-11-00075.1.

Hwang, P. A., D. M. Burrage, D. W. Wang, and J. C. Wesson (2013), Ocean surface roughness spectrum in high wind condition for microwave backscatter and emission computations, *J. Atmos. Oceanic Technol.*, *30*, 2168–2188, doi:10.1175/JTECH-D-12-00239.1.

Jackson, F. C., W. T. Walton, D. E. Hines, B. A. Walter, and C. Y. Peng (1992), Sea surface mean-square slope from Ku-band backscatter data, *J. Geophys. Res.*, *97*, 11,411–11,427.

Kahma, K. K., and C. J. Calkoen (1992), Reconciling discrepancies in the observed growth of wind-generated waves, *J. Phys. Oceanogr.*, *22*, 1389–1405, doi:10.1175/1520-0485(1992)022<1389:RDITOG>2.0.CO;2.

NASA's Ocean Biology Processing Group (2009), Distance to the nearest coast. [Available at http://oceancolor.gsfc.nasa.gov/DOCS/DistFromCoast, last accessed 13 Nov. 2015.]

National Data Buoy Center (NDBC) (1996), Nondirectional and directional wave data analysis procedures, *NDBC Tech. Doc. 96-01*. [Available at http://www.ndbc.noaa.gov/wavemeas.pdf, last accessed 1 Dec. 2015.]

National Data Buoy Center (NDBC) (2002), Non-standard acquisition times. [Available at http://www.ndbc.noaa.gov/nsacq.shtml, last accessed 6 Dec. 2015.]

National Data Buoy Center (NDBC) (2009a), At what heights are the sensors located on Moored Buoy and at C-MAN sites?. [Available at http://www.ndbc.noaa.gov/bmanht.shtml, last accessed 6 Dec. 2015.]

National Data Buoy Center (NDBC) (2009b), What are the sensors' reporting, sampling, and accuracy readings?. [Available at http://www.ndbc.noaa.gov/rsa.shtml, last accessed 6 Dec. 2015.]

National Data Buoy Center (NDBC) (2012a), Do NDBC's meteorological and oceanographic sensors measure data for the entire hour?. [Available at http://www.ndbc.noaa.gov/acq.shtml, last accessed 22 Dec. 2015.]

National Data Buoy Center (NDBC) (2012b), Wave acquisition times. [Available at http://www.ndbc.noaa.gov/waves.shtml, last accessed 6 Dec 2015.]

National Data Buoy Center (NDBC) (2015), Historical NDBC Data. [Available at http://www.ndbc.noaa.gov/historical_data.shtml, last accessed 16 Dec. 2015.]

Ruf, C. S., et al. (2012), The CYGNSS nanosatellite constellation hurricane mission, 2012 IEEE International Geoscience and Remote Sensing Symposium, Munich, pp. 214–216, doi:10.1109/IGARSS.2012.6351600.

Ruf, C., et al. (2016), New ocean winds satellite mission to probe hurricanes and tropical convection, *Bull. Am. Meteorol. Soc.*, *97*, 385–395, doi:10.1175/BAMS-D-14-00218.1.

Teng, C.-C., S. Cucullu, S. McArthur, C. Kohler, B. Burnett, and L. Bernard (2010), Vandalism of data buoys, *Mar. Weather Log*, *54*(1). [Available at http://www.vos.noaa.gov/MWL/apr_10/vandalism.shtml, last accessed 31 Dec. 2015.]

U.S. Army Coastal Engineering Research Center (CERC) (1977), *Shore Protection Manual*, vol. 1, 3rd ed.

Valenzuela, G. R. (1978), Theories for the interaction of electromagnetic and oceanic waves: A review, *Boundary Layer Meteorol.*, *13*, 61.

Weissman, D. E., W. J. Plant, and S. Stolte (1996), Response of microwave cross sections of the sea to wind fluctuations, *J. Geophys. Res.*, *101*, 12,149–12,161, doi:10.1029/96JC00558.

Young, I. R. (1998), An experimental investigation of the role of atmospheric stability in wind wave growth, *Coastal Eng.*, *34*(1–2), 23–33, doi:10.1016/S0378-3839(98)00011-8.

Young, I. R. (1999), *Wind Generated Ocean Waves*, Elsevier, Amsterdam.

Young, I. R., and L. A. Verhagen (1996), The growth of fetch limited waves in water of finite depth, Part 1. Total energy and peak frequency, *Coastal Eng.*, *29*(1–2), 47–78, doi:10.1016/S0378-3839(96)00006-3.

Zavorotny, V. U., and A. G. Voronovich (2000), Scattering of GPS signals from the ocean with wind remote sensing application, *IEEE Trans. Geosci. Remote Sens.*, *38*(2), 951–964, doi:10.1109/36.841977.